SCIENCE CHINA
Earth Sciences

•ARTICLE•

November 2023 Vol.66 No.11: 2635–2647
https://doi.org/10.1007/s11430-022-1155-6

A multidisciplinary approach in recognizing seep-carbonates: A case study from the Loiano Formation (late Eocene) in the northern Apennines (Italy)

Stefano CONTI, Filippo PANINI, Pietro PATTERI, Riccardo RONDELLI & Daniele MALFERRARI*

Department of Chemical and Geological Sciences, University of Modena and Reggio Emilia, Via Campi 103, I-41125, Modena, Italy

Received November 11, 2022; revised July 11, 2023; accepted July 27, 2023; published online October 23, 2023

Abstract Carbonate deposits related to active seeps are documented along most continental margins and are characterized by peculiar seep-related facies and by chemical (isotope signature), paleontological and mineralogical markers. Their fossil analogues are recognized all over the world by the same features and occurred since the beginning of Phanerozoic. In this paper, we present a new seep outcrop (Castagneto village, Reggio Emilia, northern Italy) belonging to the late Eocene Loiano Formation which, to our knowledge, is in Italy the most ancient seep deposit with not-reworked chemosymbiotic fauna. The outcrop can be roughly divided into two portions, a northern part showing abundant presence of macrofossils in silty carbonate matrix and sub-horizontal subdivisions, and a southern part, where macrofossils are almost absent, characterized by sub-vertical internal subdivisions and a clear vertical structure consisting of the rhythmic alternation of light and dark mineralization. Detailed analysis of samples from the southern portion showed the occurrence of authigenic calcite and pyrite, the latter with a peculiar framboidal texture. This feature, together with the occurrence of chemosymbiotic species and ^{13}C isotope depletion, suggests possible hydrocarbon-rich fluid-related genesis and provides useful criteria for identifying hydrocarbon-rich fluid-related deposits in geologic units.

Keywords Framboid, Lucinids, Methane, Pyrite, Seepage, SMTZ

Citation: Conti S, Panini F, Patteri P, Rondelli R, Malferrari D. 2023. A multidisciplinary approach in recognizing seep-carbonates: A case study from the Loiano Formation (late Eocene) in the northern Apennines (Italy). Science China Earth Sciences, 66(11): 2635–2647, https://doi.org/10.1007/s11430-022-1155-6

1. Introduction

Authigenic carbonate deposits form when hydrocarbon-rich fluids diffuse through sediments toward the seafloor (Bohrmann and Torres, 2006; Meister et al., 2008; Greinert et al., 2013; Suess, 2014), creating conditions for the development of chemosynthesis-based micro- and macro-ecosystems sustained by the energy associated with rising fluids (Aharon, 1994; Clari et al., 1994; Boetius et al., 2000; Gómez-Pérez, 2003; Baker et al., 2010). Fluid-microbial interactions is realized by the anaerobic oxidation of methane (Boetius et al., 2000) inducing the precipitation of authigenic carbonates with distinct isotopic signatures (Greinert et al., 2001). Carbonate deposits linked to active seeps are recognized along most continental margins (Baker et al., 2010) and are characterized by distinctive features (Campbell et al., 2002; Campbell, 2006): (1) discrete masses of limited extent (up to a few hundred meters) and thickness (to a few dozen meters) with peculiar seep-related facies and structures, and generally enclosed in fine-grained siliciclastic successions; (2) abundant distinctive, chemotrophic assemblages, dominated by lucinids, vesicomyids, modioloids and tube worms, but

* Corresponding author (email: daniele.malferrari@unimore.it)

absent in the enclosing sediments; (3) strong depletion of ^{13}C with $\delta^{13}C$ ranging from −15‰ to −50‰; (4) possible mineralization with peculiar textures.

Their fossil analogues have been recognized by the same features and occurred since the beginning of Phanerozoic (Campbell, 2006; Teichert and van de Schootbrugge, 2013). In the Apennine chain, seep-carbonate outcrops are mainly hosted in Neogene successions (Conti et al., 2021) and historically known under the informal lithostratigraphic name of Calcari a *Lucina* (Taviani, 1994). Seep-carbonate precipitation and fluid expulsion processes occurred in different tectonic settings of the Apennine foreland, from wedge-top basins through the outer slope of the accretionary prism, and at the leading edge of the deformational front in the inner foredeep, in correspondence of fault-related anticlines. Until now, the most ancient chemosymbiotic fauna in the northern Apennines is from the lower Miocene of the Casentino basins (Conti et al., 2017). Other older reports refer to late Oligocene ^{13}C-depleted carbonate blocks or macroconcretions (Clari et al., 2009) lacking chemosymbiotic organism remains and reworked carbonates without showing complete evidence of typical seep markers (Marroni et al., 2014).

This research presents a new seep outcrop (Castagneto village, Reggio Emilia, northern Italy) identified on the basis of seep-related facies and structures, chemosymbiotic fauna, stable isotope geochemistry and, as recently proved, by the abundant occurrence of framboidal pyrite (i.e., a microscopic spherical and subspherical aggregate of nearly equidimensional pyrite microcrystals). The presence of pyrite has long been accepted as a redox proxy in ancient (and recent) sedimentary environments (Wilkin and Barnes, 1997; Suits and Wilkin, 1998; Wignall and Newton, 1998; Wilkin and Arthur, 2001; Wignall et al., 2005, 2010; Shen et al., 2007, 2016; Zhou and Jiang, 2009; Bond and Wignall, 2010; Guan et al., 2014). Although most studies of authigenic pyrite focus primarily on pyrite content and sulfur isotopic composition (Peckmann et al., 2001; Zhang J et al., 2014; Lin et al., 2015, 2016b, 2016c; Feng et al., 2018; Liu et al., 2020b), also morphology, size, distribution and texture of pyrite crystals have been suggested as a marker of the crystallization environment (Wilkin et al., 1996; Peckmann et al., 2001; Soliman and El Goresy, 2012; Zhang M et al., 2014; Wang et al., 2015; Lin et al., 2016a; Rickard, 2019; Miao et al., 2021). Several recent studies confirmed that pyrite aggregates with framboidal texture are larger in oxic-dysoxic than in euxinic environments, promoting the presence of framboids and their size distribution as an effective marker not only of bottom water redox conditions (Wilkin et al., 1996; Wilkin and Barnes, 1997; Suits and Wilkin, 1998; Wignall and Newton, 1998; Wilkin and Arthur, 2001; Nielsen and Shen, 2004; Wignall et al., 2005, 2010; Shen et al., 2007; Zhou and Jiang, 2009; Bond and Wignall, 2010; Cavalazzi et al., 2012; Guan et al., 2014), but also as indicators of methane seepage (Lin et al., 2016a, 2016b; Rickard, 2019; Miao et al., 2021). More specifically, pyrite framboids may form and grow where the anaerobic oxidation of methane seeps and microbial reduction of sulfates occur simultaneously. This zone, normally found a few meters deep in the sediments, is known as the sulfate-methane transition zone (SMTZ) and here the formation of pyrite (and occasionally other phases) is greatly enhanced precisely because of methane infiltration (Peckmann et al., 2001; Arvidson et al., 2004; Jørgensen et al., 2004; Neretin et al., 2004; Sassen et al., 2004; Garming et al., 2005; Novosel et al., 2005; Riedinger et al., 2005; Larrasoaña et al., 2007; Lim et al., 2011; Peketi et al., 2012). Actually, in the SMTZ most of the methane gas released into the ocean is consumed by microorganisms through anaerobic oxidation coupled to sulfate/iron/manganese reduction (Knittel and Boetius, 2009) and this reaction can lead to the formation of either authigenic carbonate and pyrite, providing an important tool to study past methane seepage activities (Berner, 1984; Boetius et al., 2000; Borowski et al., 2013).

The outcrop studied in this research, which is strongly characterized by the presence of mineralization and fossils, occurs in the basal part of Epiligurian succession deposited in northern Apennine wedge-top basins indicating a late Eocene age and, to our knowledge, represents in Italy the most ancient seep deposit with not-reworked chemosymbiotic fauna. The experimental results, obtained and discussed by applying a multidisciplinary approach, outlined the geological, paleontological and mineralogical characteristics of the seepage. Seep deposits are markers of fossil fluid circulation and their identification is critical for reconstructing tectonic setting; we therefore believe that the analytical approach here proposed can be very helpful in their identification and characterization.

2. Geological setting

2.1 The northern Apennines

The orogenic wedge of the northern Apennines consists of several, imbricated tectonic units bound by thrusts generally verging to the northeast. The farthest traveled structural unit, the Ligurian nappe, presently occupies the highest position in the chain (Appendix Figure S1a, https://link.springer.com). The main component units of the nappe, the Jurassic-Eocene Ligurian units, are the remnants of the oceanic seaways of the Alpine Tethys (Ligurian Ocean) and, perhaps, of the adjacent continental margin of the Adria microplate (Bortolotti et al., 2001; Marroni and Pandolfi, 2007; Conti et al., 2020). Some of these units were deformed in a Late Cretaceous-Eocene accretionary wedge (Figure S1b), prior to the continental collision between the European plate and Adria microplate (Labaume et al., 1991; Pini, 1999; Marroni and Pandolfi, 2001; Catanzariti et al., 2007). Following the Oligocene-Miocene continental collision, clastic wedges accumulated in foreland basins in front of the deforming belt as due to the activation of crustal thrusts and the progressive roll-back of the subducting Adriatic slab (Faccenna et al., 2001; Finetti et al., 2001).

The post-collisional deformation of the western part of the Adria microplate took place during distinct tectonic phases of Oligocene, early Miocene, late Miocene, Pliocene and Pleistocene ages (Castellarin et al., 1992). These deformational phases were responsible for the onset of thrust-bounded structural units, such as the diverse Tuscan units and the Umbria-Romagna unit (Boccaletti et al., 1990; Conti and Gelmini, 1994; Vai, 2001). During the NE-ward migration of the thrust belt system, deposition occurred not only in the foredeep, but also in smaller basins located atop the internal part of the Ligurian nappe in the so-called Epiligurian succession (Ricci Lucchi and Ori, 1985; Bettelli et al., 1989). These sediments are separated by the underlying Ligurian Units by an angular unconformity of middle-late Eocene age; their deposition continued until the late Miocene, interrupted by several regional-scale unconformities (Bettelli et al., 1989; Fornaciari and Rio, 1996; Catanzariti et al., 1997; Remitti et al., 2011). Epiligurian deposits are interpreted as the infilling of thrust-top basins, which evolved during the collisional stages (wedge-top or satellite basins). During the advancement of the Ligurian nappe system, materials (sedimentary mélange, olistostromes, mass transport deposits) slide off the front of the nappe and were intercalated in foredeep deposits. Beginning in the late Oligocene, the frontal part of the Ligurian tectonic prism interacts with the inner edge of Adria (Tuscan and Umbria-Romagna units) giving rise to tectonic coverings and gravitational emplacement of materials within the slope and foredeep sequences (Conti and Fontana, 2002; Lucente and Pini, 2008; Remitti et al., 2011).

2.2 Baiso area

In the studied area (Figure 1a), the lower part of the Epiligurian succession is characterized by deposits consisting of thick accumulations of polygenic breccias (Baiso Argillaceous Breccias), marls and hemipelagic clays (Monte Piano Marls). Their age ranges from the middle Eocene (Lutetian) to early Oligocene. Enclosed in the Monte Piano Marls are present lenticular arenaceous bodies of the Loiano Fm (hereafter referred to as LOI) with an arkosic composition (Gazzi and Zuffa, 1970; Cibin, 1989). The sandstones of the LOI, represented by a confined turbidite body with complex geometry, were deposited in a deep pelagic environment below the carbonate compensation limit. They are characterized by lightly cemented whitish quartz and feldspathic siliciclastic sandstones, organized in commonly amalgamated layers and locally made up of arenaceous-pelitic turbidites in medium and thin layers. The LOI has been dated to a time interval between Lutetian and Bartonian (Bettelli et al., 2002). The studied outcrop (Figure 1b) is in the LOI near the village of Castagneto where the formation has a thickness of a few tens of meters, much lower than those of the more eastern areas (Modena and Bologna Apennines). The outcrop is part of the northern flank of a syncline involving the lower part of the Epiligurian Antognola Fm. The structure is characterized by a rather sloping southern flank with local overturns involving the Ranzano Fm that are interpreted as related to longitudinal late Oligocene inverse faults (De Nardo et al., 1992). A system of tardive extensional high-angle faults north of M. Valestra and M. S. Maria (partially coinciding with the compressive late Oligocene fault) juxtaposes (Figure 1a) the lower and the upper part (Pantano and Cigarello Fms) of the Epiligurian succession (Papani et al., 2002).

3. Samples and analytical methods

Detailed field analysis of geometry, lithology and facies conducted in the Castagneto area around the outcrop together with preliminary analysis of some samples led to the identification of two main sampling areas (Figure 1b and Figure S2a) characterized by the absence (FP4409_1 sampling area) or well noticeable occurrence (FP4409_2 sampling area) of massive sulfide mineralization and blackish patches of iron and manganese oxides and hydroxides.

All samples were characterized through classical chemical and mineralogical techniques. On a representative selection of carbonate rocks from the outcrop were collected samples for petrographic observations on thin section. Stable oxygen and carbon isotopes were measured on calcite from vein and micritic matrix. Bulk chemical and mineralogical characterization of total rock was performed on powders from three different aliquots of each sample, whereas microscopic (optical and electron) characterization was carried out on polished thin (100 μm) sections and on aliquots of disaggregated material enriched in framboids following the method proposed in Wilkin et al. (1996). More specifically, thin-section measurements were used to define the textural relationships within framboids and between framboids and other minerals, and images collected on the disaggregated material to assess the size of framboids and get size distribution. Paleontological data were derived both from the sampling performed for this research and from the analysis of fossil specimens collected in the past by the Natural Science Society of Reggio Emilia in a portion of the outcrop no longer preserved due to quarrying activities. See the Supplementary Information for further detail about instruments, analytical methods and adopted experimental conditions.

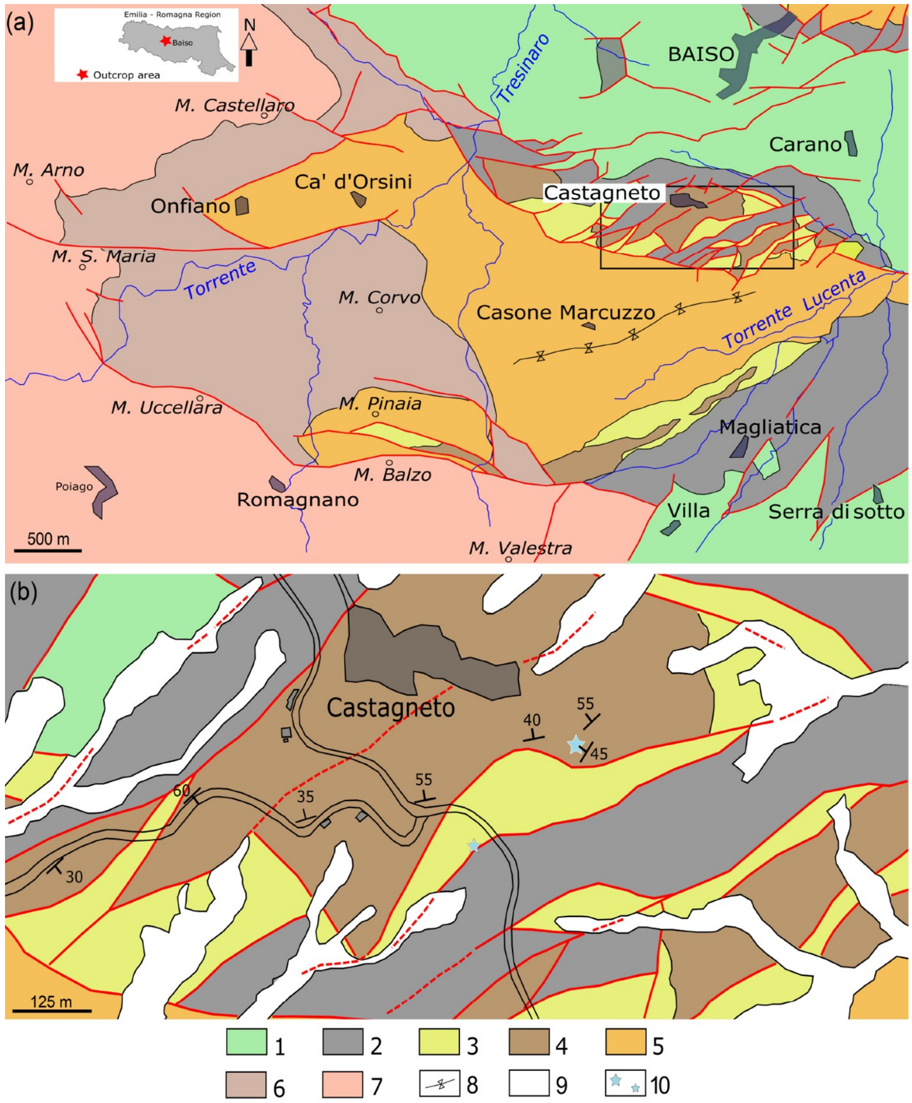

Figure 1 Geological sketch map of the Reggio Emilia Apennines south of Baiso (a) with a magnification of the outcrop area (b). Legend: (1) undifferentiated Ligurian lithostratigraphic units (Lower Cretaceous-Lower Eocene). Epiligurian Units: (2) Baiso Argillaceous Breccias (Middle/Upper Eocene); (3) Monte Piano Marls (Middle Eocene-Lower Oligocene); (4) Loiano Formation (Middle/Upper Eocene); (5) Ranzano Fm. (Lower Oligocene); (6) Antognola Fm., Val Tiepido-Canossa Argillaceous Breccias and Contignaco Fm. (Undiff.) (Upper Oligocene-Lower Miocene); (7) Pantano and Cigarello Fms. (Lower/Middle Miocene); (8) trace of sincline axial plane; (9) slope and superficial quaternary deposits; (10) studied Loiano main outcrop (big star) and isolated reworked blocks (small star). Red lines, faults; black lines, stratigraphic contacts. The black rectangle in Figure 1a identifies the area of the Castagneto outcrop enlarged in Figure 1b. Modified from Papani et al. (2002).

4. Results

4.1 Geological and paleontological overview of the outcrop

Near the small village of Castagneto, the LOI occurs showing peculiar facies and it is characterized by the absence of a clear stratification, the presence of carbonate lithologies and cements, red to black mineralization due to supergene alteration processes and abundant macro-fossiliferous content (mainly bivalves).

The Castagneto outcrop (Figure 1b, Figure S2a) has an irregularly elliptical base (about 55×40 meters in areal extension) with a thickness of about 20 m; nevertheless, historical chronicles indicate that it represents a small witness of a more extensive outcrop that was intensely exploited to produce crushed stone and mixed granulate after the second world war. Minor isolated carbonate blocks occur in the southwestern side of the studied area (Figure 1b), but they are probably reworked, as they are located near the contact between Montepiano and Ligurides. The main outcrop consists of micritic and partially laminated finely arenaceous limestones, sometimes with siliceous inclusions. Yellowish to slightly orange calcarenites are also occurring, locally brecciated and with the presence of small voids; the calcarenites, when present, are irregularly alternating with carbonate-rich sandstones and sandy levels, lithologies typical of the LOI.

Brecciated portions (Figure S2b) are irregularly pervaded by veins and sinuous conduits (Figure S2c) passing to vacuolar-vuggy-fabric with rhombohedral crystalline terminations in small geodes (Figure S2d), probably in part derived from the dissolution of organic residues. As in other Epiligurian outcrops (Conti et al., 2014), these structures are typical of seep-carbonates. Carbonate bodies are in primary position as confirmed by concordant attitudes, gradual contact, and the occurrence in the vicinity of thin seepage-related carbonate layers intercalated in the Loiano deposits.

Overall, on today's examination, the scarp represented by the residual quarry face, oriented roughly in the meridian direction, can be divided into a northern and a southern portion (roughly corresponding to sampling areas FP4409_1 and FP4409_2, respectively. The former is the only fossiliferous part and is marked by sub-horizontal subdivisions; the latter is characterized by sub-vertical internal subdivisions and by a sharp vertical structure (Figure S3) consisting of the rhythmic alternation of yellowish-white (calcite) and dark-brown to black (microcrystalline pyrite and patches of iron and manganese oxides and hydroxides) mineralization. Between the top and bottom of the vertical structure is a displacement of about 50 centimeters, imposed after the formation of the vertical structure. The anomalous lithological features, characterized by a strong carbonate content, persist even in some small exposures about twenty meters north of the main escarpment of the former quarry (traces of possible original stratification are still present in them). Residues of fluid seepage are also clearly visible in thin section; in fact, the compositional lithological imprinting of the LOI appears to be pervaded by a regular pattern of veins and fractures with an evident presence of metallic mineralization (Figure 2a) that will be later described. As will be reported below a distinctive feature of the samples from the Castagneto outcrop is that, despite the presence of iron oxides/hydroxides, pyrite was almost always found forming framboids of well-preserved crystals.

Fossil remains abundantly occur especially in the central part of the northern portion, roughly corresponding to the old quarry floor. These are complete models (internal and external, or composites), mainly of bivalves and gastropods sometimes mineralized to form small calcite geodes (Figure S4a). More specifically, samples collected for this study revealed the presence of bivalves (lucinids), in isolated and/or not densely-clustered specimens; nevertheless, there is evidence (samples stored at the repository of the Natural Science Society of Reggio Emilia) also of an abundant and often densely-clustered past seep-fauna. Bivalves are predominant and belong mainly to the subfamily *Bathymodiolinae* and to the Families *Lucinidae* and *Vesicomyidae*, for which chemosymbiosis or close relation to chemosynthetic food chain can be reliably inferred and considered characteristic of seep-communities (Kiel and Taviani, 2017; Hryniewicz, 2022). Also associated are specimens of *Solemyidae* (*Acharax*), which are common, but not exclusive, to the same environments, as they are adapted to anoxic conditions. It is also known that *Solemyidae*, *Lucinidae* and *Vesicomyidae* belong to a sulfide-based community (Le Pennec et al., 1995; Taylor and Glover, 2013); in particular, *Vesicomyidae* (Figure S4a) are likely to be associated with high levels of sulfide (Taviani, 1994; Glover and Taylor, 2007). In addition, even among the numerous specimens found in the past by members of the Natural Science Society of Reggio Emilia, monospecific concentrations of the bivalves of these groups appear only rarely. On the contrary, dense and chaotic assemblages of several species, including a few gastropods (*Buccinidae*, *Colinae* subfamily), are more common. These groupings of fossils (Figure S4b), together with the presence of sandy veils within the limestone and of *Bathymodiolinae* and *Lucinidae* in isolated valves (Figure S4c), could result from local rearrangements caused by low-energy fluid expulsion phases. Trace of tubeworms (Annelida Polychaetes) and sporadic poorly preserved remains interpretable as decapod crustacean are also present along with other fossil remains of problematic determination. Fossiliferous patches are associated with bioturbation traces and burrows. At the base of the outcrop, some calcareous blocks with stromatolitic fabric and some decimetric globular nodules with calcite veins resembling a septaria-like structure were noted, as reported in other outcrops of ancient cold seeps (Krajewski and Luks, 2003; Cavalazzi, 2005).

A comprehensive taxonomic study of the seep-fauna (made particularly challenging by the presence of endemics and new species and, not least, by the difficulty in isolating individual specimens) is underway.

4.2 Bulk mineralogical and chemical characterization

X-ray powder diffraction (XRPD) measurements (Figure S5), primarily carried out to define the sampling areas described above, well show the occurrence of pyrite, gypsum and calcite only in the samples collected from area FP4409_2, thus confirming the observations made in outcrop. In the samples from area FP4409_1, sulfide and sulfate are not detectable; in contrast, quartz, feldspar, illite, dolomite and calcite are well represented, with significant differences in concentration depending on the sampling point. These phases are also confirmed by the chemical analysis of the major elements and by the sulfur content (Table S1).

4.3 Isotopic analyses

The negative δ^{13}C signature of the carbonates is recognized as the best evidence of a methane-related origin, whereas δ^{18}O signature providing information on the temperature of

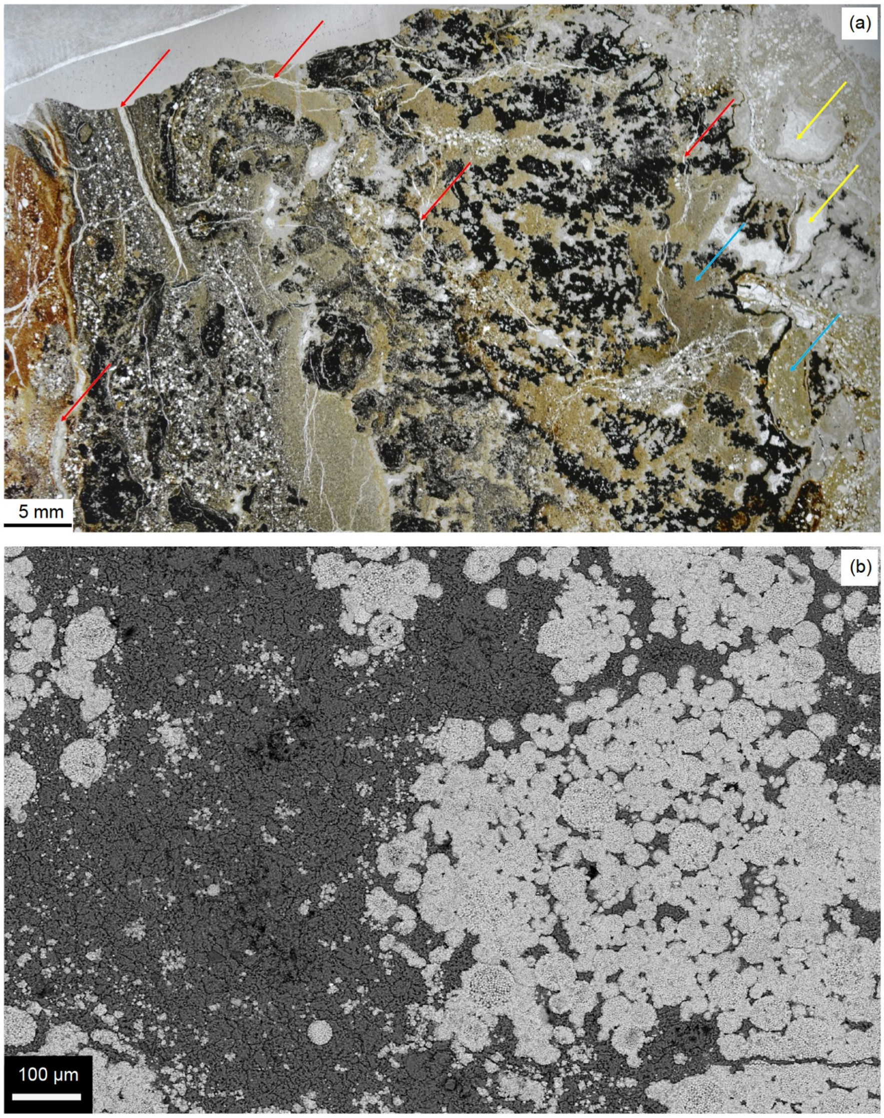

Figure 2 (a) Detail of a thin section with occurrence of filled fractures (red arrows), pyrite framboids (blue arrows) and calcite grains (yellow arrows). (b) Representative SEM image (general overview) of pyrite framboids both isolated and aggregated to form clusters of different sizes and geometry.

seep carbonate precipitation and on the origin of fluids (Aloisi et al., 2000; Chang et al., 2022; Yao et al., 2022).

Samples of carbonate material for $\delta^{13}C$ and $\delta^{18}O$ measurements were taken from two types of carbonate material, microcrystalline matrix and veins (as, for example, indicated in Figure 2a by the yellow and red arrows, respectively). Samples from area FP4409_2 showed $\delta^{13}C$ values (Table S2) ranging from −34.3‰ to −6.2‰ (matrix) and −32.5‰ to −13.6‰ (veins), with a median of −28.1‰ (matrix) and −27.6‰ (veins) and standard deviations (SD) of 8.3‰ (matrix) and 6.1‰ (veins). Samples from area FP4409-1 show averagely higher $\delta^{13}C$ values ranging from −29.5‰ to −5.4‰ (matrix) and −26.8‰ to −10.0‰ (veins), with a median of −21.4‰ (matrix) and −18.2‰ (veins) and SD of 7.6‰ (matrix) and 6.1‰ (veins). $\delta^{18}O$ values are broadly similar for all sample types and range from: (1) −3.9‰ to −0.45‰ (matrix) and −3.5‰ to −1.0‰ (veins), with a median of −1.7‰ (matrix and vein) and SD of 0.86‰ (matrix) and 0.84‰ (veins) in area FP4409_2; (2) −3.0‰ to −0.98‰ (matrix) and −3.7‰ to −1.2‰ (veins), with a median of −1.5‰ (matrix) and −2.2‰ (veins) and SD of 0.50‰ (matrix) and 0.79‰ (veins) in area FP4409_1.

4.4 Scanning electron microscopy

In samples not mineralized with sulfides (sampling area FP4409_1), in agreement with XRPD measurements, the most occurring phases are quartz, illite, calcite and, to a lesser extent, dolomite (Figure S6); occasionally zircon and barite/celestine crystals have also been observed.

In samples from area FP4409_2, according to preliminary optical microscopy observations, and as evidenced by the low magnification SEM image shown in Figure 2b, pyrite framboids are the dominant textural form. As will be detailed below, the framboids are both isolated and aggregated to form clusters of different sizes and geometry; although rarer, isolated pyrite crystals with octahedral habit were also observed. Gypsum and carbonates are present, among the latter mainly calcite as evidenced by XRPD (Figure S5b), but also, tough rarely, dolomite, the latter not detectable by XRPD. Quartz and feldspar relicts, oxide/hydroxide particle and small crystals of barite (very rare) can also be observed, but in such quantities that they are not detected by XRPD (oxides/hydroxides could not be detected because they are probably amorphous).

Framboids (Figure 3a, 3b) consist of several microcrystals generally subhedral, but sometimes exhibit pyritohedral (Figure 3c) or octahedral (Figure 3d) habit; the latter usually protrudes from the external surface of the framboid. The arrangement of individual pyrite crystallites within framboids is normally disordered, although in some cases pyrite microcrystals follow nearly regular concentric patterns (Figure 3e, yellow dashed circle) or form "sub-framboids" within larger framboids (Figure 3f, yellow dashed circles). It is also notable that the individual pyrite crystals inside the framboids, unlike at the edge, are typically isolated from each other. The size of microcrystals showing pyritohedral habit is fairly homogeneous and varies between about 3 and 4 μm (Figure 3c).

Both isolated framboids (Figure 4a, 4b), but mostly aggregated to form clusters of various sizes and geometry (e.g., Figure 4c), were observed. The external (pseudo) spherical shape of the framboids is almost unaltered; nevertheless, even if rarely, the aggregates show polygonal contours with flattening at their edges in correspondence to contacts with other surrounding framboids (Figure 4c). Isolated octahedral pyrite crystals (e.g., Figure 4b) are occasionally found in different parts of the rock without, however, following a precise textural pattern. Pocket-like structures formed by the aggregation of more or less deformed framboids closely compacted with each other also occur (Figure 4d, 4e). Inside these pockets may be found single framboids, relicts of

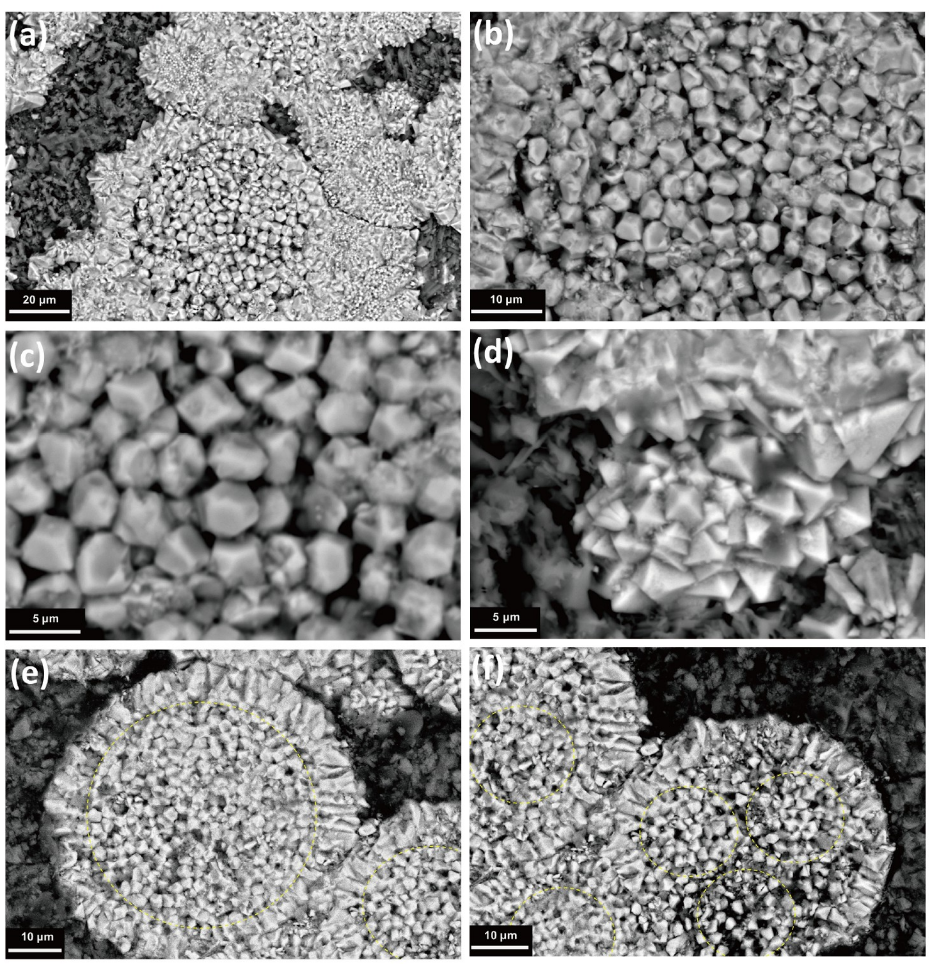

Figure 3 SEM images showing the morphology and structure of individual pyrite crystals within the framboid ((a), magnified in (b)). Pyrite microcrystals can sometimes exhibit pyritohedral ((c), magnification of (a)) or octahedral (d) habit; crystallites occasionally form nearly regular concentric patterns (e) or "sub-framboids" within larger framboids (f) as marked by the yellow dashed circles.

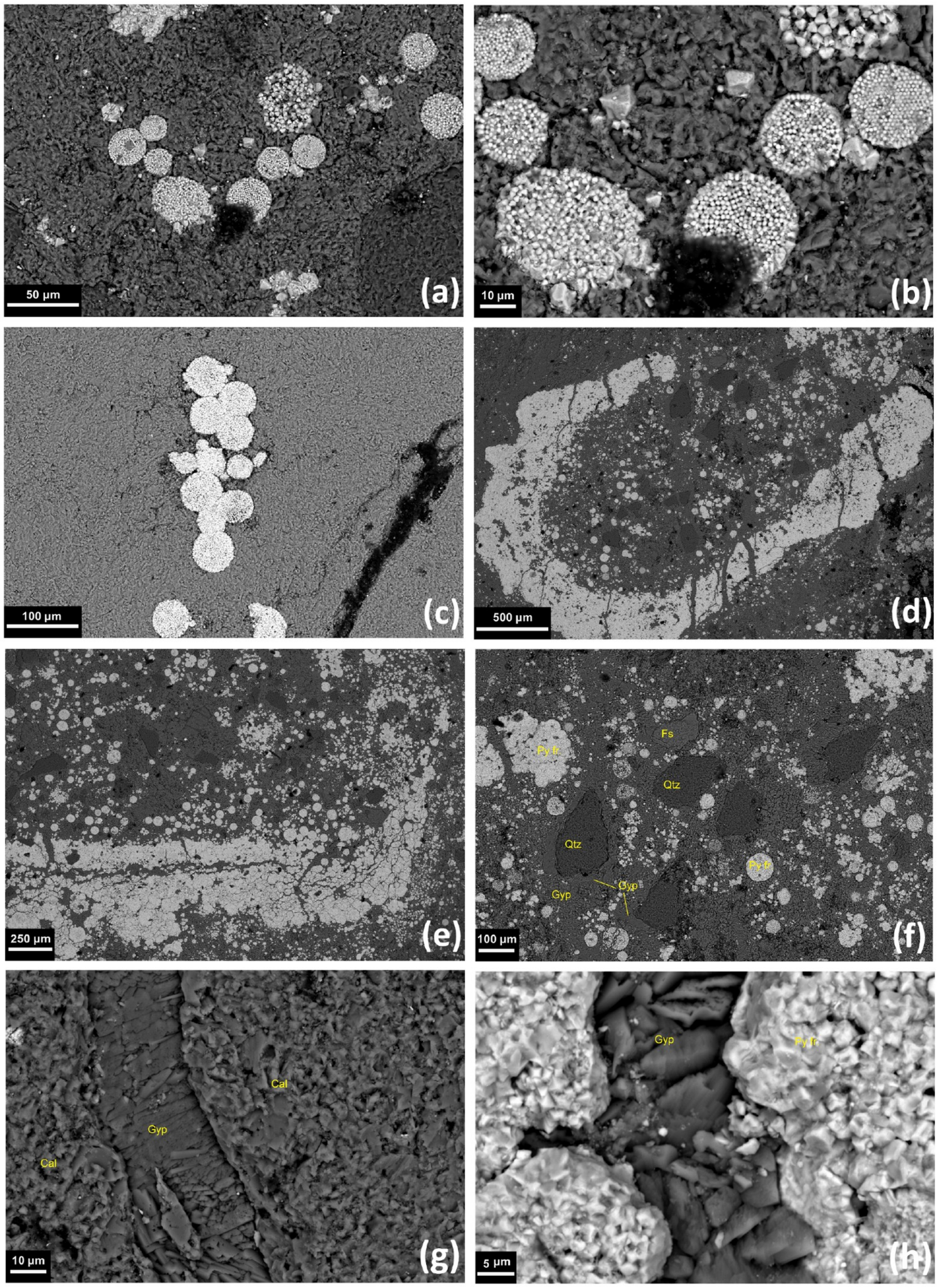

Figure 4 SEM images of isolated ((a), and enlarged in (b)) and clustered framboids (c); pocket-like structures formed by the aggregation of framboids ((d), (e)) "hosting" other framboids and relics of quartz and feldspar (f); gypsum veins between calcite (g) or pyrite framboids (h). Isolated pyrite crystals with octahedral habit (b) are also visible.

quartz and feldspar frequently wrapped in a gypsum matrix (Figure 4f); as mentioned above, quartz and feldspars were not detected by XRPD, but their (modest) occurrence is confirmed also by chemical analysis (Table S1). The gypsum was also found to form thin, elongated veins between calcite (Figure 4g) and framboids (Figure 4h).

The interstitial material between/within pyrite framboids is like those in the pockets. Iron oxides and/or hydroxides form irregularly shaped, isolated structures of modest size (Figure S7) and elongated structures of varying shape and size (>250 microns, Figure S8); in both cases, they are always within a carbonate (calcite and low-Mg calcite) matrix. Although it is conceivable that they derive from the alteration of pyrite, other genetic mechanisms cannot be ruled out, since we have never found them associated with pyrite relics and/or showing significant sulfur contents.

The sizes of pyrite framboids are obtained from five different samplings collected in the FP4409_2 area with higher pyrite concentration. Analysis of the size distribution (Figure 5) shows that the mean diameter (MD) of framboidal pyrite varies from 4.3 to 77.1 μm with a mean value of 37.2 μm and a SD of 14.7 μm, thus indicating a significant difference in the size distribution.

5. Discussion

Methane seepage and associated faunal communities in the Apennine chain are reported from the early Miocene onwards (Conti et al., 2017; Kiel and Taviani, 2017). Among them, Miocene seep deposits essentially contains large bathymodiolin, vesicomyid and lucinid bivalves, whereas the sporadic Pliocene outcrops reveal similarities with modern restricted Mediterranean seep fauna (Taviani, 1994; Cau et al., 2015; Oppo et al., 2015). The only deposit with an age comparable with the Castagneto outcrop is the middle Eocene Buje deposit (Natalicchio et al., 2015), but in a very different geological context. In this scenario the Castagneto outcrop represents a peculiar situation in the LOI: chemosymbiotic fauna, seep-related facies, isotope analyses and framboidal pyrite suggest that carbonates were formed as a consequence of anaerobic oxidation of methane. The southern part of the outcrop, dominated by sub-vertical discontinuities and traces of seep ducts, could represent the main, rather fast, rising point of the fluids. Vertical lineaments, breccias, fractures and conduits resemble plumbing structures reported in fossil mud volcanoes (Clari et al., 2004), suggesting a similar origin for this portion of the Castagneto outcrop, related to rapid and vigorous fluid emission. The northern part, characterized by sub-horizontal lithofacies subdivisions and with a significant presence of fossil remains, would instead represent a sector with slower and more widespread emissions. The occurrence of brecciated/dislocated bodies and of infiltration conducts in the southern part (Figures S2 and S3) agrees with the seepage scenario and suggests partly piped fluid transport rather than pervasive infiltration; in fact, mineralization is well concentrated in small areas and quickly fades in nonmineralized calcarenites. This aspect also agrees with observations made in the past in other sedimentary basins interested by infiltration (Conti and Fontana, 2002; Clari et al., 2004; Zwicker et al., 2021; Yao et al., 2022).

High concentration of framboidal pyrite can be considered as a signal to identify the position of the SMTZ in the stratigraphic column. More specifically, in an anoxic environment, methane in sediments can undergo strong sulfate-driven anaerobic oxidation that occurs exactly in the sulfate reduction zone, resulting in the formation of framboidal pyrite (Sassen et al., 2004; Lin et al., 2016a, 2016b, 2016c). In the Castagneto outcrop the contacts between the various framboids rarely are flattened, with some minor exceptions (e.g., Figure 4c) or when they are closely aggregated to form the pocket-like structures (Figure 4d, 4e). This feature probably indicates absence (or low) plasticity at the time of formation. The aggregation of framboids of various sizes suggest the presence of cavities of various dimensions at the time of crystallization. The absence of textures other than framboidal (single octahedral pyrite crystals are present, but rare) suggest their formation in a single event or, at least, during a succession of single, rapid and close pulses that led the pyrite framboids to undergo successive stages of overgrowth, as evidenced by the occurrence of "sub-framboids" within larger framboids (Figure 3f). In addition, the pyrite microcrystals within each framboid have approximately the same size denoting that nucleation and growth occurred simultaneously, thus strengthening the hypothesis of a single (or rapid pulsed) genetic event. More complex is the explanation of the occurrence of pocket-like structures. We believe it is unlikely that these are fossil casts, especially because of their irregular and uneven shape evidenced in various samples. The most likely hypothesis is that these are natural cavities that are common in other outcrops of the LOI (although not mineralized).

Gypsum veins among the framboids (Figure 4h) indicate conditions of sulfur supersaturation during their formation; however, it cannot be completely ruled out that the gypsum formed, even in recent times, in an aerial environment by sulfide dissolution and subsequent re-precipitation of the sulfate (although no pyrite relics associated with iron oxides were found in the thin sections, reddish discolorations correlating with sulfide alteration are clearly evident on the outcrop rocks, Figure S3). The presence of a non-negligible amount of magnesium in the samples from the FP4409-2 area and the absence of diffuse dolomite (i.e., not detected by XRPD) suggest the occurrence of low-magnesium calcite rather than pure calcite. Indeed, the occurrence of dissolved sulfide catalyzes the dehydration of magnesium by promoting the precipitation of Mg-calcite (Smrzka et al., 2020).

Pyrite can form either in the water column in euxinic conditions, or diagenetically within the sediment. In the first case, the crystals precipitate rather rapidly and once covered by sediment they no longer growth. On the other hand, crystals formed in a diagenetic environment can increase in size depending on element availability and redox conditions. This difference in genetic mechanism means that pyrite crystals (and aggregates) that form diagenetically are normally larger and more heterogeneously sized than syngenetic ones (Wilkin et al., 1996; Wilkin and Barnes, 1997; Bond and Wignall, 2010; Wignall et al., 2010). Statistical studies (Wilkin et al., 1996; Wilkin and Barnes, 1997; Bond and Wignall, 2010) of the size of pyrite framboids in recent marine sediments performed, however, without considering the sulfate-driven anaerobic oxidation of methane, showed that in a sulfide marine environment the crystallization of numerous small framboids with mean diameter (MD) less than 6 μm and a very small SD is favored; in contrast, in an oxidizing environment the framboids are fewer in number, but larger in size (MD>6 μm) and show high SD values (usually higher than 3 μm). Subsequently, Lin et al. (2016b), based on samples collected in recent sediments on the northern continental slope of the South China Sea demonstrated that in the SMTZ, the size and size distribution of pyrite framboids could be boosted by the anaerobic oxidation of methane (AOM) which promote not only the formation of large pyrite framboids (average diameter greater than 20 μm), but also their aggregation into clusters. Lin et al. (2016b) also concluded that pyrite textures, originated where only sulfate reduction occurred, are different; therefore, the presence of textures with large and heterogeneous framboids can be considered a valid marker in paleo-marine systems of high AOM conditions. Similar conclusions were reached by Miao et al. (2021) studying authigenic pyrite in the sediments of site Q6 of "Haima seep" (Qiongdongnan Basin, South China Sea, China). The considerations that can be drawn from the analysis of the size distributions of pyrite framboids (Figure 5) parallel those of the authors mentioned earlier, thus strengthening the hypothesis that framboids formed under AOM conditions confirming methane seepages. Whether or not the nucleation of the framboids was mediated by organic matter prior to the methane seeps is unknown. However, the conspicuous occurrence of framboids also with large size suggests that there was an abundant, perhaps pulsed, supply of iron and hydrogen sulfide from the seepage; this allowed pyrite to continue to grow/aggregate into framboids of various sizes even depending on the space (cavities) available. In contrast, in normal marine sedimentary environments, where "normal" sulfate reduction occurs, the rate of pyrite formation is usually lower (Liu et al., 2019, 2020a).

Isotopic measurements made on the carbonates indicate that the carbon has a methanogenic origin, and the carbonates can be assumed to be in "textural equilibrium" with pyrite, further strengthening the hypothesis that precipitation was induced by AOM coupled with sulfate reduction. In fact, values of $\delta^{13}C<-25‰$ indicate a substantial contribution of methane-carbon to the isotopic footprint of calcite (Aloisi et al., 2000; Chang et al., 2022; Yao et al., 2022). The absence of substantial changes in both $\delta^{13}C$ and $\delta^{18}O$ between micritic matrix and veins suggests that calcite solubilized from surrounding sediments is probably recrystallized in the veins. Although the lowest values of $\delta^{13}C$ are for samples with the greatest pyrite mineralization, no gradual transition from low to high values is observed where mineralization does not occur or where there is no evidence of seep-related structure (northern part of the outcrop). Negative values greater than −25‰ do not discriminate with certainty the presence of seep (Chang et al., 2022); however, in the area of the Castagneto outcrop, which is very modest in size, seepage is also likely to have affected, although less extensively, the northern part

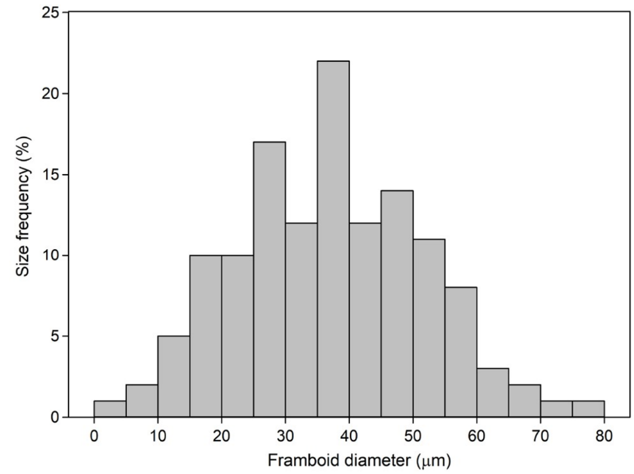

Figure 5 Frequency histogram of size distribution of framboidal pyrite calculated on 131 framboids from five samplings.

where mineralization are not evident and where $\delta^{13}C$ values are averagely higher than −25‰.

Interactions with meteoric fluids can reduce both $\delta^{13}C$ and $\delta^{18}O$ (Marshall, 1992; Kaufman and Knoll, 1995), and correlations between $\delta^{13}C$ and $\delta^{18}O$ values are documented in the literature (e.g., Chang et al., 2022; Yao et al., 2022). In samples from the Castagneto outcrop, assuming micritic calcite as representative of the host rock, no correlations between the two isotopes are observed (Figure S9). The high $\delta^{18}O$ values found for all samples are in apparent contrast to the lithological characteristics of the area which has considerable brecciation (thus potentially favorable for alteration by meteoric water). However, they agree with the homogeneity of $\delta^{13}C$ values found in veins and matrix, suggesting that the original isotopic signature (seepage and cold deep-sea waters of the LOI environment) has not been substantially altered.

The outcrops of the LOI of the Reggio Emilia Apennines represent the western end of a turbiditic basin that developed for at least seventy kilometers longitudinally with respect to the actual chain. The depocentral areas are located eastward in the Bologna Apennines where the formation probably exceeds a thousand meters in thickness. Towards the west, in the Parma and Piacenza Apennines, the LOI is not present. This situation suggests that the basin was largely controlled by syn-depositional tectonics which maintained highly structural areas where the sedimentation of arenaceous turbidites was inhibited or extremely reduced, and areas of constant subsidence, where considerable thicknesses of siliciclastic turbiditic materials (i.e., the LOI) could accumulate. The fault systems activated in this context could thus represent the preferential pathway for methane seepage, probably sourced from the potential reservoirs represented by the less clayey portions (Cretaceous and Tertiary turbiditic sequences) of the Ligurian accretionary prism underlying the Epiligurian succession and already extensively tectonized during the Ligurian or Mesoalpine tectonic phase (middle Eocene).

6. Conclusion

This study, carried out by applying a multi-analytical and multidisciplinary approach, outlines the geological, paleontological and mineralogical feature of a very rare if not unique seep outcrop belonging to the Loiano Formation. The detailed facies and samples analyses showed that authigenic pyrite found in the Castagneto outcrop crystalized under methane seepage activity. Although these results refer to a small outcrop, they are in nice agreement with other research conducted on larger areas also in recent sedimentary environments, thus suggesting that the occurrence of framboids in ancient marine deposits can not only be considered as an indicator of increasing AOM, but also defines the position of the SMTZ in the paleo-marine system. We want to reiterate that the identification of the seep system is crucial for reconstructing plumbing system as, in northern Apennines, is generally linked to the tectonic setting.

Acknowledgements *We thank Daniela MANZINI from the Scientific Instruments Facility of the University of Modena and Reggio Emilia, Federico LUGLI (University of Modena and Reggio Emilia) and Paola IACUMIN (University of Parma) for assistance during isotopic measurements. We are very grateful to the Natural Science Society of Reggio Emilia (Reggio Emilia, Italy) for providing fossiliferous material. This work was supported by the FAR UniMORE 2022-2023 Funding.*

References

Aharon P. 1994. Geology and biology of modern and ancient submarine hydrocarbon seeps and vents: An introduction. Geo-Mar Lett, 14: 69–73

Aloisi G, Pierre C, Rouchy J M, Foucher J P, Woodside J. 2000. Methane-related authigenic carbonates of eastern Mediterranean Sea mud volcanoes and their possible relation to gas hydrate destabilisation. Earth Planet Sci Lett, 184: 321–338

Arvidson R S, Morse J W, Joye S B. 2004. The sulfur biogeochemistry of chemosynthetic cold seep communities, gulf of Mexico, USA. Mar Chem, 87: 97–119

Baker M C, Ramirez-Llodra E Z, Tyler P A, German C R, Boetius A, Cordes E E, Dubilier N, Fisher C R, Levin L A, Metaxas A, Rowden A A, Santos R S, Shank T M, Van Dover C L, Young C M, Warén A. 2010. Biogeography, ecology, and vulnerability of chemosynthetic ecosystems in the deep sea. In: McIntyre A, ed. Life in the World's Oceans: Diversity, Distribution, and Abundance. Oxford: Wiley-Blackwell. 161–182

Berner R A. 1984. Sedimentary pyrite formation: An update. Geochim Cosmochim Acta, 48: 605–615

Bettelli G, Bonazzi U, Fazzini P, Panini F. 1989. Schema introduttivo alla geologia delle Epiliguridi dell'Appennino modenese e delle aree limitrofe. Mem Soc Geol Ital, 39: 215–246

Bettelli G, Panini F, Pizziolo M, Bonazzi U, Capitani M, Fazzini P, Fioroni C, Fregni P, Gasperi G, Mantovani Uguzzoni MP, Bosi R, Fontana D. 2002. Note illustrative della Carta Geologica d'Italia alla scala 1:50.000 foglio illustrativo 236 Pavullo nel Frignano

Boccaletti M, Calamita F, Deiana G, Gelati R, Massari F, Moratti G, Ricci Lucchi F. 1990. Migrating foredeep-thrust belt systems in the northern Apennines and southern Alps. Palaeogeogr Palaeoclimatol Palaeoecol, 77: 3–14

Boetius A, Ravenschlag K, Schubert C J, Rickert D, Widdel F, Gieseke A, Amann R, Jørgensen B B, Witte U, Pfannkuche O. 2000. A marine microbial consortium apparently mediating anaerobic oxidation of methane. Nature, 407: 623–626

Bohrmann G, Torres M E. 2006. Gas hydrates in marine sediments. In: Schulz H D, Zabel M, eds. Marine Geochemistry. Berlin, Heidelberg: Springer. 481–512

Bond D P G, Wignall P B. 2010. Pyrite framboid study of marine Permian-Triassic boundary sections: A complex anoxic event and its relationship to contemporaneous mass extinction. GSA Bull, 122: 1265–1279

Borowski W S, Rodriguez N M, Paull C K, Ussler III W. 2013. Are ^{34}S-enriched authigenic sulfide minerals a proxy for elevated methane flux and gas hydrates in the geologic record? Mar Pet Geol, 43: 381–395

Bortolotti V, Principi G, Treves B. 2001. Ophiolites, Ligurides and the tectonic evolution from spreading to convergence of a Mesozoic Western Tethys segment. In: Vai G B, Martini I P, eds. Anatomy of an Orogen: The Apennines and Adjacent Mediterranean Basins. Dordrecht: Springer Netherlands. 151–164

Campbell K A, Farmer J D, Des Marais D. 2002. Ancient hydrocarbon seeps from the Mesozoic convergent margin of California: Carbonate geochemistry, fluids and palaeoenvironments. Geofluids, 2: 63–94

Campbell K A. 2006. Hydrocarbon seep and hydrothermal vent paleoenvironments and paleontology: Past developments and future research directions. Palaeogeogr Palaeoclimatol Palaeoecol, 232: 362–407

Castellarin A, Cantelli L, Fesce A M, Mercier J L, Picotti V, Pini G A, Prosser G, Selli L. 1992. Alpine compressional tectonics in the southern Alps: Relationships with the N-Apennines. Ann Tectonicae, 6: 62–94

Catanzariti R, Ellero A, Levi N, Ottria G, Pandolfi L. 2007. Calcareous nannofossil biostratigraphy of the Antola Unit succession (Northern Apennines, Italy): New age constraints for the Late Cretaceous Helminthoid Flysch. Cretac Res, 28: 841–860

Catanzariti R, Rio D, Martelli L. 1997. Late Eocene to Oligocene calcareous nannofossil biostratigraphy in Northern Appennines: The Ranzano Sandstone. Mem Soc Geol Ital, 49: 207–253

Cau S, Franchi F, Roveri M, Taviani M. 2015. The Pliocene-age Stirone River hydrocarbon chemoherm complex (Northern Apennines, Italy). Mar Pet Geol, 66: 582–595

Cavalazzi B, Barbieri R, Cady S L, George A D, Gennaro S, Westall F, Lui A, Canteri R, Rossi A P, Ori G G, Taj-Eddine K. 2012. Iron-framboids in the hydrocarbon-related Middle Devonian Hollard Mound of the Anti-Atlas mountain range in Morocco: Evidence of potential microbial biosignatures. Sediment Geol, 263-264: 183–193

Cavalazzi B. 2005. L'attività microbica in rocce carbonatiche prodotte in ecosistemi chemiosintetici: Documentazione fossile e potenziale di preservazione. Paleoitalia, 13: 36–42

Chang B, Huang J, Algeo T J, Pancost R D, Wan X, Xue Y, Jia J, Wang Z, Hu J, Wang J, Wang S, Wu J, Xie S. 2022. Episodic massive release of methane during the mid-Cretaceous greenhouse. GSA Bull, 134: 2958–2970

Cibin U. 1989. Petrografia e provenienza delle Arenarie di Loiano (Eocene sup. - Oligocene inf., Appennino bolognese e modenese). G Geol, 51: 81–92

Clari P, Cavagna S, Martire L, Hunziker J. 2004. A Miocene mud volcano and its plumbing system: A chaotic complex revisited (Monferrato, NW Italy). J Sediment Res, 74: 662–676

Clari P, Dela Pierre F, Martire L, Cavagna S. 2009. The Cenozoic CH_4-derived carbonates of Monferrato (NW Italy): A solid evidence of fluid circulation in the sedimentary column. Mar Geol, 265: 167–184

Clari P, Fornara L, Ricci B, Zuppi G M. 1994. Methane-derived carbonates and chemosymbiotic communities of Piedmont (Miocene, northern Italy): An update. Geo-Mar Lett, 14: 201–209

Conti P, Cornamusini G, Carmignani L. 2020. An outline of the geology of the Northern Apennines (Italy), with geological map at 1:250,000 scale. Int J Geosci, 139: 149–194

Conti S, Argentino C, Fioroni C, Salocchi A C, Fontana D. 2021. Miocene seep-carbonates of the Northern Apennines (Emilia to Umbria, Italy): An overview. Geosciences, 11: 53
Conti S, Fioroni C, Fontana D. 2017. Correlating shelf carbonate evolutive phases with fluid expulsion episodes in the foredeep (Miocene, northern Apennines, Italy). Mar Pet Geol, 79: 351–359
Conti S, Fontana D, Lucente C C, Pini G A. 2014. Relationships between seep-carbonates, mud volcanism and basin geometry in the Late Miocene of the northern Apennines of Italy: The Montardone mélange. Int J Earth Sci-Geol Rund, 103: 281–295
Conti S, Fontana D. 2002. Sediment instability related to fluid venting in Miocene authigenic carbonate deposits of the northern Apennines (Italy). Int J Earth Sci-Geol Rund, 91: 1030–1040
Conti S, Gelmini R. 1994. Miocene-Pliocene tectonic phases and migration of foredeep-thrust belt system in Northern Apennines. Memorie Società Geologica Italiana, 48: 261–274
De Nardo M T, Iaccarino S, Martelli L, Papani G, Tellini C, Torelli L, Vernia L. 1992. Osservazioni sull'evoluzione del bacino satellite epiligure Vetto-Carpineti-Canossa (Appennino Settentrionale). Mem Descr Carta Geol D'Italia, XLVI: 209–220
Faccenna C, Becker T W, Lucente F P, Jolivet L, Rossetti F. 2001. History of subduction and back-arc extension in the Central Mediterranean. Geophys J Int, 145: 809–820
Feng D, Qiu J W, Hu Y, Peckmann J, Guan H, Tong H, Chen C, Chen J, Gong S, Li N, Chen D. 2018. Cold seep systems in the South China Sea: An overview. J Asian Earth Sci, 168: 3–16
Finetti I R, Boccaletti M, Bonini M, Del Ben A, Geletti R, Pipan M, Sani F. 2001. Crustal section based on CROP seismic data across the North Tyrrhenian-Northern Apennines-Adriatic Sea. Tectonophysics, 343: 135–163
Fornaciari E, Rio D. 1996. Latest Oligocene to early-middle Miocene quantitative calcareous nannofossil biostratigraphy in the Mediterranean region. Micropaleontology, 42: 1
Garming J F L, Bleil U, Riedinger N. 2005. Alteration of magnetic mineralogy at the sulfate-methane transition: Analysis of sediments from the Argentine continental slope. Phys Earth Planet Inter, 151: 290–308
Gazzi P, Zuffa G G. 1970. Le arenarie paleogeniche dell'Appennino emiliano. Minerlogica Petrogr Acta, 16: 97–137
Glover EA, Taylor JD. 2007. Diversity of chemosymbiotic bivalves on coral reefs: Lucinidae (Mollusca, Bivalvia) of New Caledonia and Lifou. Zoosystema, 29: 109–181
Gómez-Pérez I. 2003. An Early Jurassic deep-water stromatolitic bioherm related to possible methane seepage (Los Molles Formation, Neuquén, Argentina). Palaeogeogr Palaeoclimatol Palaeoecol, 201: 21–49
Greinert J, Bohrmann G, Suess E. 2001. Gas hydrate-associated carbonates and methane-venting at hydrate ridge: Classification, distribution, and origin of authigenic lithologies. In: Natural Gas Hydrates: Occurrence, Distribution, and Detection. American Geophysical Union (AGU). 99–113
Greinert J, Bohrmann G, Suess E. 2013. Gas hydrate-associated carbonates and methane-venting at hydrate ridge: Classification, distribution, and origin of authigenic lithologies. In: Paull C K, Dillon W P, eds. Geophysical Monograph Series. Washington, D. C.: American Geophysical Union. 99–113
Guan C, Zhou C, Wang W, Wan B, Yuan X, Chen Z. 2014. Fluctuation of shelf basin redox conditions in the early Ediacaran: Evidence from Lantian Formation black shales in South China. Precambrian Res, 245: 1–12
Hryniewicz K. 2022. Ancient seep carbonates: From outcrop appearance to microscopic petrography. In: Kaim A, Cochran J K, Landman N H, eds. Ancient Hydrocarbon Seeps. Vol. 53. Topics in Geobiology. Cham: Springer International Publishing. 79–110
Jørgensen B B, Böttcher M E, Lüschen H, Neretin L N, Volkov I I. 2004. Anaerobic methane oxidation and a deep H_2S sink generate isotopically heavy sulfides in Black Sea sediments. Geochim Cosmochim Acta, 68: 2095–2118
Kaufman A, Knoll A. 1995. Neoproterozoic variations in the C-isotopic composition of seawater: Stratigraphic and biogeochemical implications. Precambrian Res, 73: 27–49
Kiel S, Taviani M. 2017. Chemosymbiotic bivalves from Miocene methane-seep carbonates in Italy. J Paleontol, 91: 444–466
Knittel K, Boetius A. 2009. Anaerobic oxidation of methane: Progress with an unknown process. Annu Rev Microbiol, 63: 311–334
Krajewski K, Luks B. 2003. Origin of "cannon-ball" concretions in the Carolinefjellet Formation (Lower Cretaceous), Spitsbergen. Pol Polar Res 24: 217–242
Labaume P, Berty C, Laurent P. 1991. Syn-diagenetic evolution of shear structures in superficial nappes: An example from the Northern Apennines (NW Italy). J Struct Geol, 13: 385–398
Larrasoaña J C, Roberts A P, Musgrave R J, Gràcia E, Piñero E, Vega M, Martínez-Ruiz F. 2007. Diagenetic formation of greigite and pyrrhotite in gas hydrate marine sedimentary systems. Earth Planet Sci Lett, 261: 350–366
Le Pennec M, Beninger P G, Herry A. 1995. Feeding and digestive adaptations of bivalve molluscs to sulphide-rich habitats. Comp Biochem Physiol Part A-Physiol, 111: 183–189
Lim Y C, Lin S, Yang T F, Chen Y G, Liu C S. 2011. Variations of methane induced pyrite formation in the accretionary wedge sediments offshore southwestern Taiwan. Mar Pet Geol, 28: 1829–1837
Lin Q, Wang J, Algeo T J, Sun F, Lin R. 2016a. Enhanced framboidal pyrite formation related to anaerobic oxidation of methane in the sulfate-methane transition zone of the northern South China Sea. Mar Geol, 379: 100–108
Lin Q, Wang J S, Fu S Y, Lu H F, Bu Q T, Lin R X, Sun F. 2015. Elemental sulfur in northern South China Sea sediments and its significance. Sci China Earth Sci, 58: 2271–2278
Lin Q, Wang J, Taladay K, Lu H, Hu G, Sun F, Lin R. 2016b. Coupled pyrite concentration and sulfur isotopic insight into the paleo sulfate–methane transition zone (SMTZ) in the northern South China Sea. J Asian Earth Sci, 115: 547–556
Lin Z, Sun X, Peckmann J, Lu Y, Xu L, Strauss H, Zhou H, Gong J, Lu H, Teichert B M A. 2016c. How sulfate-driven anaerobic oxidation of methane affects the sulfur isotopic composition of pyrite: A SIMS study from the South China Sea. Chem Geol, 440: 26–41
Liu J, Pellerin A, Antler G, Kasten S, Findlay A J, Dohrmann I, Røy H, Turchyn A V, Jørgensen B B. 2020a. Early diagenesis of iron and sulfur in Bornholm Basin sediments: The role of near-surface pyrite formation. Geochim Cosmochim Acta, 284: 43–60
Liu J, Pellerin A, Izon G, Wang J, Antler G, Liang J, Su P, Jørgensen B B, Ono S. 2020b. The multiple sulphur isotope fingerprint of a sub-seafloor oxidative sulphur cycle driven by iron. Earth Planet Sci Lett, 536: 116165
Liu X, Fike D, Li A, Dong J, Xu F, Zhuang G, Rendle-Bühring R, Wan S. 2019. Pyrite sulfur isotopes constrained by sedimentation rates: Evidence from sediments on the East China Sea inner shelf since the late Pleistocene. Chem Geol, 505: 66–75
Lucente C C, Pini G A. 2008. Basin-wide mass-wasting complexes as markers of the Oligo-Miocene foredeep-accretionary wedge evolution in the Northern Apennines, Italy. Basin Res, 20: 49–71
Marroni M, Molli G, Pandolfi L, pertusati P. 2014. The relationships between northern Apennine and western Alps: State of the art fifty years after The"Ruga Del Bracco. Pisa: Proceedings of the Meeting in Memory of Piero Elter. 79
Marroni M, Pandolfi L. 2001. Debris flow and slide deposits at the top of the Internal Liguride ophiolitic sequence, Northern Apennines, Italy: A record of frontal tectonic erosion in a fossil accretionary wedge. Isl Arc, 10: 9–21
Marroni M, Pandolfi L. 2007. The architecture of an incipient oceanic basin: A tentative reconstruction of the Jurassic Liguria-Piemonte basin along the Northern Apennines-Alpine Corsica transect. Int J Earth Sci-Geol Rund, 96: 1059–1078
Marshall J D. 1992. Climatic and oceanographic isotopic signals from the carbonate rock record and their preservation. Geol Mag, 129: 143–160
Meister P, Bernasconi S M, Vasconcelos C, McKenzie J A. 2008. Sealevel

changes control diagenetic dolomite formation in hemipelagic sediments of the Peru Margin. Mar Geol, 252: 166–173

Miao X, Feng X, Liu X, Li J, Wei J. 2021. Effects of methane seepage activity on the morphology and geochemistry of authigenic pyrite. Mar Pet Geol, 133: 105231

Natalicchio M, Peckmann J, Birgel D, Kiel S. 2015. Seep deposits from northern Istria, Croatia: A first glimpse into the Eocene seep fauna of the Tethys region. Geol Mag, 152: 444–459

Neretin L N, Böttcher M E, Jørgensen B B, Volkov I I, Lüschen H, Hilgenfeldt K. 2004. Pyritization processes and greigite formation in the advancing sulfidization front in the upper Pleistocene sediments of the Black Sea. Geochim Cosmochim Acta, 68: 2081–2093

Nielsen J K, Shen Y. 2004. Evidence for sulfidic deep water during the Late Permian in the East Greenland Basin. Geology, 32: 1037–1040

Novosel I, Spence G D, Hyndman R D. 2005. Reduced magnetization produced by increased methane flux at a gas hydrate vent. Mar Geol, 216: 265–274

Oppo D, Capozzi R, Picotti V, Ponza A. 2015. A genetic model of hydrocarbon-derived carbonate chimneys in shelfal fine-grained sediments: The Enza River field, Northern Apennines (Italy). Mar Pet Geol, 66: 555–565

Papani G, De Nardo M T, Bettelli G, Rio D, Tellini C, Vernia L. 2002. Note Illustrative della Carta Geologica d'Italia alla scala 1:50.000, Foglio 218 "Castelnuovo ne' Monti"

Peckmann J, Reimer A, Luth U, Luth C, Hansen B T, Heinicke C, Hoefs J, Reitner J. 2001. Methane-derived carbonates and authigenic pyrite from the northwestern Black Sea. Mar Geol, 177: 129–150

Peketi A, Mazumdar corresponding author A, Joshi R K, Patil D J, Srinivas P L, Dayal A M. 2012. Tracing the Paleo sulfate-methane transition zones and H_2S seepage events in marine sediments: An application of C-S-Mo systematics. Geochem Geophys Geosyst, 13, http://doi.org/10.1029/2012GC004288

Pini G A. 1999. Tectosomes and olistostromes in the argille scagliose of Northern Apennines, Italy. Geological Society of America. U.S.A.

Remitti F, Vannucchi P, Bettelli G, Fantoni L, Panini F, Vescovi P. 2011. Tectonic and sedimentary evolution of the frontal part of an ancient subduction complex at the transition from accretion to erosion: The case of the Ligurian wedge of the northern Apennines, Italy. GSA Bull, 123: 51–70

Ricci Lucchi F, Ori G. 1985. Field excursion D: Syn-orogenic deposits of a migrating basin system in the NW Adriatic Forelan. In: Allen P H, Homewood P, Williams G, eds. Excursion guidebook. Foreland Basins Symposium. Fribourg. 137–176

Rickard D. 2019. Sedimentary pyrite framboid size-frequency distributions: A meta-analysis. Palaeogeogr Palaeoclimatol Palaeoecol, 522: 62–75

Riedinger N, Pfeifer K, Kasten S, Garming J F L, Vogt C, Hensen C. 2005. Diagenetic alteration of magnetic signals by anaerobic oxidation of methane related to a change in sedimentation rate. Geochim Cosmochim Acta, 69: 4117–4126

Sassen R, Roberts H H, Carney R, Milkov A V, DeFreitas D A, Lanoil B, Zhang C. 2004. Free hydrocarbon gas, gas hydrate, and authigenic minerals in chemosynthetic communities of the northern Gulf of Mexico continental slope: Relation to microbial processes. Chem Geol, 205: 195–217

Shen J, Feng Q, Algeo T J, Li C, Planavsky N J, Zhou L, Zhang M. 2016. Two pulses of oceanic environmental disturbance during the Permian-Triassic boundary crisis. Earth Planet Sci Lett, 443: 139–152

Shen W, Lin Y, Xu L, Li J, Wu Y, Sun Y. 2007. Pyrite framboids in the Permian-Triassic boundary section at Meishan, China: Evidence for dysoxic deposition. Palaeogeogr Palaeoclimatol Palaeoecol, 253: 323–331

Smrzka D, Feng D, Himmler T, Zwicker J, Hu Y, Monien P, Tribovillard N, Chen D, Peckmann J. 2020. Trace elements in methane-seep carbonates: Potentials, limitations, and perspectives. Earth-Sci Rev, 208: 103263

Soliman M F, El Goresy A. 2012. Framboidal and idiomorphic pyrite in the upper Maastrichtian sedimentary rocks at Gabal Oweina, Nile Valley, Egypt: Formation processes, oxidation products and genetic implications to the origin of framboidal pyrite. Geochim Cosmochim Acta, 90: 195–220

Suess E. 2014. Marine cold seeps and their manifestations: Geological control, biogeochemical criteria and environmental conditions. Int J Earth Sci-Geol Rund, 103: 1889–1916

Suits N S, Wilkin R T. 1998. Pyrite formation in the water column and sediments of a meromictic lake. Geology, 26: 1099–1102

Taviani M. 1994. The "calcari a Lucina" macrofauna reconsidered: Deep-sea faunal oases from Miocene-age cold vents in the Romagna Apennine, Italy. Geo-Mar Lett, 14: 185–191

Taylor J, Glover E. 2013. New lucinid bivalves from shallow and deeper water of the Indian and West Pacific Oceans (Mollusca, Bivalvia, Lucinidae). ZooKeys, 326: 69–90

Teichert B M A, van de Schootbrugge B. 2013. Tracing Phanerozoic hydrocarbon seepage from local basins to the global Earth system. Palaeogeogr Palaeoclimatol Palaeoecol, 390: 1–3

Vai GB. 2001. Structure and stratigraphy: An overview. In: Vai G B, Martini I P, eds. Anatomy of an Orogen: The Apennines and Adjacent Mediterranean Basins. Dordrecht: Springer Netherlands. 15–31

Wang M, Cai F, Li Q, Liang J, Yan G J, Dong G, Wang F, Shao H B, Hu G W. 2015. Characteristics of authigenic pyrite and its sulfur isotopes influenced by methane seep at Core A, Site 79 of the middle Okinawa Trough. Sci China Earth Sci, 58: 2145–2153

Wignall P B, Bond D P G, Kuwahara K, Kakuwa Y, Newton R J, Poulton S W. 2010. An 80 million year oceanic redox history from Permian to Jurassic pelagic sediments of the Mino-Tamba terrane, SW Japan, and the origin of four mass extinctions. Glob Planet Change, 71: 109–123

Wignall P B, Newton R, Brookfield M E. 2005. Pyrite framboid evidence for oxygen-poor deposition during the Permian-Triassic crisis in Kashmir. Palaeogeogr Palaeoclimatol Palaeoecol, 216: 183–188

Wignall P B, Newton R. 1998. Pyrite framboid diameter as a measure of oxygen deficiency in ancient mudrocks. Am J Sci, 298: 537–552

Wilkin R T, Arthur M A. 2001. Variations in pyrite texture, sulfur isotope composition, and iron systematics in the Black Sea: Evidence for Late Pleistocene to Holocene excursions of the O_2-H_2S redox transition. Geochim Cosmochim Acta, 65: 1399–1416

Wilkin R T, Barnes H L, Brantley S L. 1996. The size distribution of framboidal pyrite in modern sediments: An indicator of redox conditions. Geochim Cosmochim Acta, 60: 3897–3912

Wilkin R T, Barnes H L. 1997. Formation processes of framboidal pyrite. Geochim Cosmochim Acta, 61: 323–339

Yao H, Chen X, Brunner B, Birgel D, Lu Y, Guo H, Wang C, Peckmann J. 2022. Hydrocarbon seepage in the mid-Cretaceous greenhouse world: A new perspective from southern Tibet. Glob Planet Change, 208: 103683

Zhang J, Lei H Y, Ou W J, Yang Y F, Gong C J, Shi C X. 2014. Research of the sulfate-methane transition zone (SMTZ) in sediments of 973-4 column in continental slope of Northern South China Sea. Nat Gas Geosci 25: 1811–1820

Zhang M, Konishi H, Xu H, Sun X, Lu H, Wu D, Wu N. 2014. Morphology and formation mechanism of pyrite induced by the anaerobic oxidation of methane from the continental slope of the NE South China Sea. J Asian Earth Sci, 92: 293–301

Zhou C, Jiang S Y. 2009. Palaeoceanographic redox environments for the lower Cambrian Hetang Formation in South China: Evidence from pyrite framboids, redox sensitive trace elements, and sponge biota occurrence. Palaeogeogr Palaeoclimatol Palaeoecol, 271: 279–286

Zwicker J, Smrzka D, Steindl F, Böttcher M E, Libowitzky E, Kiel S, Peckmann J. 2021. Mineral authigenesis within chemosynthetic microbial mats: Coated grain formation and phosphogenesis at a Cretaceous hydrocarbon seep, New Zealand. Depositional Record, 7: 294–310

(Editorial handling: Maoyan ZHU)